Supporting Information for: Impact of Shell Growth on Recombination Dynamics and Exciton-Phonon Interaction in CdSe-CdS Core-Shell Nanoplatelets

Alexander W. Achtstein,[*,†] Oliver Marquardt,[‡] Riccardo Scott,[†] Mohamed Ibrahim,[†] Thomas Riedl,[¶] Anatol V. Prudnikau,[§,‖] Artsiom Antanovich,[§] Nina Owschimikow,[†] Jörg K.N. Lindner,[¶] Mikhail Artemyev,[§] and Ulrike Woggon[†]

[†]*Institute of Optics and Atomic Physics, Technical University of Berlin, Strasse des 17. Juni 135, 10623 Berlin, Germany*

[‡]*Weierstrass Institute for applied analysis and Stochastics, Mohrenstraße 39, 10117 Berlin, Germany*

[¶]*Department of Physics, Paderborn University, Warburger Strasse 100, 33098 Paderborn , Germany*

[§]*Research Institute for Physical Chemical Problems of Belarusian State University, 220006, Minsk, Belarus*

[‖]*Physical Chemistry, TU Dresden, Bergstrasse 66b, 01062 Dresden, Germany*

E-mail: achtstein@tu-berlin.de

Fax: +49(0)30 31421079

TEM Characterization and Absorption Spectra

In Figure S1 we show the TEM characterization of the 4.5 ML CdSe-2 ML and 3 ML CdS shell CdSe-CdS samples in addition to the TEM images of the core only and 1 ML samples in Figure 1 (c) of the main text. The growth of a 3 ML CdS shell is substantiated by the total

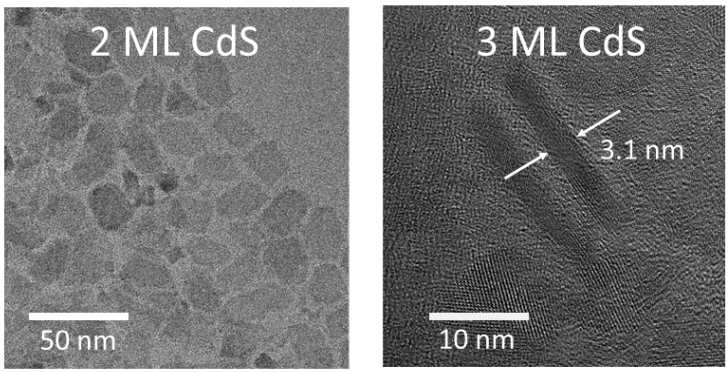

Figure S1: Transmission electron micrographs of the used 4.5 ML CdSe core only and 2 ML and 3 ML CdS shell CdSe-CdS samples.

thickness of the platelet (3.1 nm), which agrees well with a total thickness of 4.5 ML CdSe and $2 \cdot 3$ ML CdS yielding 3.11 nm, where we used the monolayer thicknesses obtained as the half lattice parameter, which is listed in Table S1 below. As mentioned in the methods section, the lateral size of the 3 ML CdS shell particles is 18x22 nm^2, while the initial CdSe core-only platelet was 8-9x10 nm^2. Figure S2 shows the absorption spectra of the used 4.5 ML CdSe core only and 1-3 ML CdS shell samples.

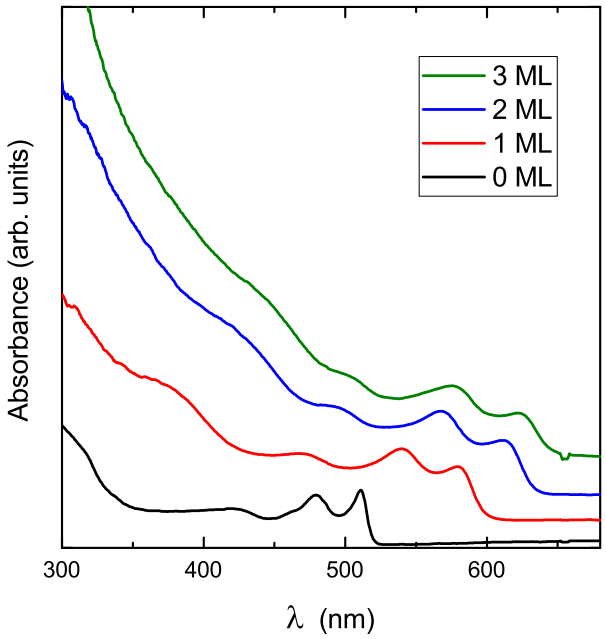

Figure S2: Absorption spectra (stacked) of 4.5 ML core-only and 1 to 3 ML (CdS) CdSe-CdS core-shell nanoplatelets at 300 K (b). Clearly a redshift of the lowest exciton transition is observed as in the PL spectra in Figure 1 (b) of the main text.

Rate equation model

Following Ref. 1 we model the time resolved dynamics in CdSe core-only and CdSe-n ML CdS nanoplatelets by the means of coupled rate equations. The level scheme of an excited and ground state is depicted in Fig. S3 and represented by the following rate equations for all occurring radiative and non-radiative transitions

$$\dot{n}_{ES} = -n_{ES}\left(\Gamma^r_{ES} + \Gamma^{nr}_{ES} + \gamma_0\left(n_\Delta + 1\right)\right) + n_{GS}\gamma_0 n_\Delta \tag{S1}$$

$$\dot{n}_{GS} = -n_{GS}\left(\Gamma^r_{GS} + \Gamma^{nr}_{GS} + \gamma_0 n_\Delta\right) + n_{ES}\gamma_0\left(n_\Delta + 1\right) \tag{S2}$$

with n_i, with i =ES or GS, the state populations, $\Gamma^r_{ES,GS}$ the radiative and $\Gamma^{nr}_i = \Gamma^{nr,0}_i + \Gamma^{nr,00}_i e^{-\Delta E^t_i/k_bT}$ the nonradiative decay rate (constants) and $n_\Delta = (e^{\Delta E/k_bT} - 1)^{-1}$ a Bose occupation statistics factor. $\Delta E = 25.6\,\text{meV}$ is the energy difference of both emissive states taken from the core sample at zero temperature. γ_0 is the zero temperature ES $\rightarrow$ GS scattering rate. Equations S1 and S2 form a system of coupled first order differential equations,

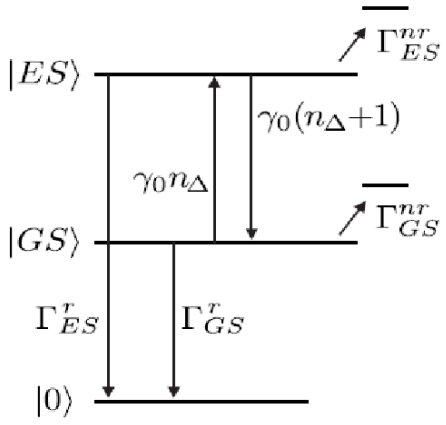

Figure S3: Level scheme of CdSe nanoplatelet emitters: The PL emission consist of an excited state and ground state exciton emission.

which can be solved by calculating the state eigenvectors.

$$\begin{aligned} \dot{n}_{ES} &= A\, n_{ES} + B\, n_{GS} \\ \dot{n}_{GS} &= C\, n_{ES} + D\, n_{GS} \end{aligned} \tag{S3}$$

With the matrix elements:

$$\begin{aligned} A &= -\Gamma^r_{ES} - \Gamma^{nr}_{ES} - (1+n_\Delta)\,\gamma_0 \\ B &= n_\Delta \gamma_0 \\ C &= (1+n_\Delta)\,\gamma_0 \\ D &= -\Gamma^r_{GS} - \Gamma^{nr}_{GS} - n_\Delta \gamma_0 \end{aligned} \tag{S4}$$

and eigenvalues:

$$\lambda_{1/2} = \frac{A+D}{2} \mp \sqrt{\frac{A^2}{4} + \frac{D^2}{4} + BC - \frac{AD}{2}} \tag{S5}$$

λ_1 and λ_2 are negative and $\lambda_1 < \lambda_2$, so we attribute λ_2 as the slow and λ_1 as the fast decay rate, referred to in the main text as $-\lambda_S$ and $-\lambda_F$, respectively.

We asssume $n_{GS}(t=0) = n_{ES}(t=0)$ as initial condition to find our Eigenvectors, as

after photoexcitation, carrier cooling and exciton formation occur on a time scale faster than our time resolution limit.[2] The evolution of the PL signal from ES and GS is given in equations S6 and S6. I_0 is a proportionality factor representing the collection efficiency and sensitivity of our setup. We obtain:

$$I_{ES}(t) = I_0\Gamma^r_{ES}n_{ES}(t) = I_0\Gamma^r_{ES}n^{(t=0)}_{ES}\left[e^{\lambda_1 t} + \frac{\overbrace{\frac{C}{\lambda_1 - D} - 1}^{f}}{1 - \frac{C}{\lambda_2 - D}}e^{\lambda_2 t}\right] \tag{S6}$$

$$I_{GS}(t) = I_0\Gamma^r_{GS}n_{GS}(t) = I_0\Gamma^r_{GS}n^{(t=0)}_{GS}\left[\underbrace{\frac{C}{\lambda_1 - D}}_{g}e^{\lambda_1 t} + \underbrace{\frac{C}{\lambda_2 - D}\frac{\frac{C}{\lambda_1 - D} - 1}{1 - \frac{C}{\lambda_2 - D}}}_{h}e^{\lambda_2 t}\right] \tag{S7}$$

Bi-exponential decays with identical decay constants λ_1 and λ_2 for ES and GS, but with different amplitudes (1,f, g and h) are obtained. Our global fit model also allows to express the experimentally accessible time integrated PL ratio of ES to GS emission with the parameters of the rate equation system for the core-only platelet sample. The time integrated luminescence of ES and GS is obtained by integrating $I_{ES}(t)$ and $I_{GS}(t)$ over time. Taking the ratio $R^{TI-PL}_{ES,GS}(T)$ of these two quantities eliminates the proportionality factor I_0:

$$R^{TI-PL}_{ES,GS}(T) = \frac{\int_0^\infty I_{ES}(t)dt}{\int_0^\infty I_{GS}(t)dt} = \frac{\Gamma^r_{ES}}{\Gamma^r_{GS}} \cdot \frac{\lambda_1^{-1} + f\lambda_2^{-1}}{g\lambda_1^{-1} + h\lambda_2^{-1}} \tag{S8}$$

Hence we can fit the intensity ratio R in our fit model with globally shared parameters for the CdSe core-only sample. For the CdS coated samples this ratio cannot be evaluated as broadening does not allow for a separation of ES and GS PL intensities. But since we have also measured the time integrated PL emission of our samples versus temperature, and this figure of merit is sensitive to the actual non-radiative recombination too, we express the

time integrated sum of ES and GS emission (T.I.) as

$$T.I. = I_{ES+GS}^{TI-PL} = \int_0^\infty I_{ES}(t)dt + \int_0^\infty I_{GS}(t)dt = S_0[\Gamma_{ES}^r(\lambda_f^{-1} + f\lambda_s^{-1}) + \Gamma_{GS}^r(g\lambda_f^{-1} + h\lambda_s^{-1})] \quad \text{(S9)}$$

This quantity is also fitted in our global approach in Figure 4 (main text) with shared parameters for each sample. The temperature dependence of the fast and slow decay constants (λ_F and λ_S) and time integrated PL (T.I.) as well as the time integrated PL intensity ratio $R_{ES,GS}^{TI-PL}(T)$ can then be globally (simultaneously) fitted, i.e. sharing the temperature dependent parameters A, B, C and D (as defined above). The introduction of the non-radiative decay channels in our rate equation model is justified due to the fact that the PL quantumyield is finite in any sample. For all CdS coated samples we find $\Gamma_i^{nr,0} = 0$, for the CdSe-core-only sample we find with $\Gamma_i^{nr,0} = 1/\text{ns}$, a finite zero temperature non-radiative rate, which may be attributed the not as good passivation without a CdS shell. The activation energies were considered as equal for ES and GS and range from 11 meV (core-only) to 16 meV (Core-Shell), reflecting a better passivation by the CdS shell due to a higher activation barrier for non-radiative processes. The 1 ML sample has with $\Gamma_{GS}^{nr,00} = 12/\text{ns}$ and $\Gamma_{ES}^{nr,00} = 98/\text{ns}$ higher zero temperature non-radiative rates, which may be the result of a not as good sample quality as compared to the other samples, reflected, e.g., in the faster decay as compared to the 2 ML sample. This is also in line with the order of magnitude lower intensity at 4 K at the end of the window in Figure 3 (b) as compared to the core-only sample (a).

Simulations

We have computed the ground state electronic properties of the systems under consideration using an eight-band $\mathbf{k} \cdot \mathbf{p}$ model, taking strain, piezoelectricity, and excitonic effects into account.[3] The elastic properties of the system were computed using linear elasticity theory[4] and both formalisms were implemented within the Sphinx-software library.[5,6] The ligand

was simulated without its influence on the elastic properties of the CdSe/CdS platelet. The potential barriers imposed by the ligand were realized by its HOMO-LUMO-gap. To quantify the impact of different contributions to the electronic properties, we have subsequently increased the amount of contributions in our simulations. In the first step, simulations have been performed taking only bulk electronic properties into account. Second, strain and piezoelectric potentials were taken into account. Finally, we have incorporated ground state electron-hole interaction self-consistently within the Hartree approximation.[7] The respective transition energies between the electron and hole ground states, Ψ_e and Ψ_h are shown as a function of the thickness of the CdS shell in Fig. 5 (main text).

The CdS shell has a significant influence on the transition energies. Strain and excitonic effects have a significant influence on the electronic properties. Generally, the computed energies (at zero temperature) agree well with the measured data for T=4 K. We note that piezoelectric potentials are of the order of a few meV with their extrema outside of the CdSe core such that their influence on the electron and hole ground states is negligible. However, this conclusion is not necessarily valid for excited states. The ground state charge densities of electron and hole are shown for the core-only system and for a CdSe platelet with a 3 ML thick CdS shell in Fig. 5 (b) (main text). While most of the charge density is inside the CdSe core, a visible nonzero charge density in the ligand or CdS shell remains.

To quantify the contribution of electron-hole recombination outside the CdSe core, we have computed the ground state electron-hole overlap as $\mathcal{O} = |\langle\Psi_\mathrm{e}|\Psi_\mathrm{h}\rangle|^2$. (See main text table 1) Also the respective percentage of electron-hole overlaps inside the CdSe core, the CdS shell and the ligand are shown there for the different thicknesses of the CdS shell. In all cases, more than 95% of the overlap result from the CdSe core. However, a small amount is leaking into the ligand in the case of the core-only system. This is significantly reduced by introduction of the CdS shell, already at a thickness of 1 ML. However, for the systems with 1, 2, and 3 ML thick CdS shells, the percentage of electron-hole overlap inside the CdS shell is in the order of a few per cent.

The following table includes the used physical constants for the simulations of CdS and CdSe-CdS nanoplatelets.

Table S1: Lattice and elastic, piezoelectric and dielectric, and electronic band structure parameters employed for our simulations. If not indicated otherwise, parameters are taken from Ref. 8. a: Ref. 9. b: Ref. 10. c: Ref. 11. The ligand work function of 4.60 eV was taken from Ref. 12 and the activation energy from Ref. 13.

Parameter	CdSe	CdS
a (Å)	6.052	5.832
C_{11} (GPa)[a]	88.1	97.8
C_{12} (GPa)[a]	53.6	59.7
C_{44} (GPa)[a]	27.4	30.6
e_{14} (C/m^2)[b]	0.16	0.29
κ[c]	9.5	8.43
E_g (eV)	1.732	2.50
m_e (m_0)	0.11	0.25
γ_1	3.265	2.721
γ_2	1.162	0.841
γ_3	1.443	1.152
Δ_{so}	0.42	0.065
E_P (eV)	16.5	21.0
a_c (eV)	-2.8324	-2.7781
a_v (eV)	1.1487	1.608
b (eV)	-1.0476	1.0912
d (eV)	-3.10	-3.50

Quantumyield

Our above mentioned rate equation model lets us also obtain the temperature dependent quantumyield of the samples. Defined as the sum of the population decaying radiatively devided by the sum of populations decaying radiatively and non-radiatively, we integrate the population decay over time using the definitions in equations S3 and S4 from above:

$$\begin{aligned}
\eta^{TR-PL}(T) &= \frac{N^r_{ES}+N^r_{GS}}{N^r_{ES}+N^r_{GS}+N^{nr}_{ES}+N^{nr}_{GS}} \\
&= \frac{\int_0^\infty \left(n_{ES}\Gamma^r_{ES}+n_{GS}\Gamma^r_{GS}\right)dt}{\int_0^\infty \left(n_{ES}\Gamma^r_{ES}+n_{GS}\Gamma^r_{GS}+n_{ES}\Gamma^{nr}_{ES}+n_{GS}\Gamma^{nr}_{GS}\right)dt} \\
&= \frac{\Gamma^r_{ES}(\lambda_f^{-1}+f\lambda_s^{-1})+\Gamma^r_{GS}(g\lambda_f^{-1}+h\lambda_s^{-1})}{(\Gamma^r_{ES}+\Gamma^{nr}_{ES})(\lambda_f^{-1}+f\lambda_s^{-1})+(\Gamma^r_{GS}+\Gamma^{nr}_{GS})(g\lambda_f^{-1}+h\lambda_s^{-1})}
\end{aligned} \tag{S10}$$

According to equations S7 and S6 it can be shown that the total population decaying through a radiative or nonradiative channel of ES or GS is $N^{r,nr}_{ES,GS} = \int_0^\infty (\dot{N}^{r,nr}_{ES,GS})dt = \int_0^\infty n_{ES,GS}\Gamma^{r,nr}_{ES,GS}dt$, with the radiative channel (r) and non-radiative channel (nr). The above expression takes the changing populations of ES and GS into account, and hence provides an exact measure for the nanoparticle's quantumyield. The results are shown for exemplary samples in Figure 6 of the main text using the parameters obtained from the global analysis. Please note that terms including γ_0 only contribute implicitly *via* f, g, and h, but not directly, as no population is destroyed by the inter-level scattering.

Equation S10 is quite complicated with respect to the above defined parameters f, g, and h, so we compare the result with a simpler approximation, for CW excitation. In the steady state case (TI) it can be shown that Equation S10 turns into the simple expression

$$\eta^{TI}(T) = \frac{\Gamma^r_{ES}+\Gamma^r_{GS}}{\Gamma^r_{ES}+\Gamma^r_{GS}+\Gamma^{nr}_{ES}+\Gamma^{nr}_{GS}}. \tag{S11}$$

It should be noted that this QY is still temperature dependent *via* the temperature dependent non-radiative rates $\Gamma^{nr}_{ES,GS}(T)$, given above in this Supporting Information. Figure 6 (main text) shows, that Equation S11 is a good approximation within a few percent error for our nanoplatelets. We remark that this equation resembles well known expressions[14]

$$\eta^{PL}(T) = \frac{1}{1 + C\, e^{-E_A/k_b T}} \tag{S12}$$

if equal activation energies are assumed for ES and GS and $\Gamma_i^{nr,0} = 0$, with $C = (\Gamma^{nr}_{ES} + \Gamma^{nr}_{GS})/(\Gamma^{r}_{ES} + \Gamma^{r}_{GS})$ the ratio of non-radiative to radiative rates turns into $C = (\Gamma^{nr} + \Gamma^{nr})$ $/(\Gamma^{r} + \Gamma^{r}) = 2\Gamma^{nr}/2\Gamma^{r} = \Gamma^{nr}/\Gamma^{r}$ if the two states are degenerate. We further note that eqs.S10 and S11 are measures for the systems quantum yield and are not to be confused with the time integrated luminescence signal of eq. S9.

References

1. Achtstein, A. W.; Scott, R.; Kickhöfel, S.; Jagsch, S. T.; Christodoulou, S.; Bertrand, G. H.; Prudnikau, A. V.; Antanovich, A.; Artemyev, M.; Moreels, I.; Schliwa, A.; Woggon, U. p-State Luminescence in CdSe Nanoplatelets: Role of Lateral Confinement and a Longitudinal Optical Phonon Bottleneck. *Phys. Rev. Lett.* **2016**, *116*, 116802.

2. Sippel, P.; Albrecht, W.; van der Bok, J. C.; Van Dijk-Moes, R. J. a.; Hannappel, T.; Eichberger, R.; Vanmaekelbergh, D. Femtosecond Cooling of Hot Electrons in CdSe Quantum-Well Platelets. *Nano Lett.* **2015**, *15*, 2409–2416.

3. Enders, P.; Bärwolff, A.; Woerner, M.; Suisky, D. k·p Theory of Energy Eands, Wave Functions, and Optical Selection Rules in Strained Tetrahedral Semiconductors. *Phys. Rev. B* **1995**, *51*, 16695–16704.

4. Povolotskyi, M.; der Maur, M. A.; Carlo, A. D. Strain Effects in Freestanding Three-Dimensional Nitride Nanostructures. *Phys. Stat. Sol. C* **2005**, *2*, 3891–3894.

5. Boeck, S.; Freysoldt, C.; Dick, A.; Ismer, L.; Neugebauer, J. The Object-Oriented DFT Program Library S/PHI/nX. *Comput. Phys. Commun.* **2011**, *182*, 543 – 554.

6. Marquardt, O.; Boeck, S.; Freysoldt, C.; Hickel, T.; Schulz, S.; Neugebauer, J.; O'Reilly, E. P. A Generalized Plane-Wave Formulation of k·p Formalism and Continuum-Elasticity Approach to Elastic and Electronic Properties of Semiconductor Nanostructures. *Comput. Mat. Sci.* **2014**, *95*, 280 – 287.

7. Stier, O.; Grundmann, M.; Bimberg, D. Electronic and Optical Properties of Strained Quantum Dots Modeled by 8-Band k·p Theory. *Phys. Rev. B* **1999**, *59*, 5688–5701.

8. Bose, S.; Song, Z.; Fan, W. J.; Zhang, D. H. Effect of Lateral Size and Thickness on the Electronic Structure and Optical Properties of Ouasi Two-Dimensional CdSe and CdS Nanoplatelets. *J. Appl. Phys.* **2016**, *119*, 143107.

9. Deligoz, E.; Colakoglu, K.; Ciftci, Y. Elastic, Electronic, and Lattice Dynamical Properties of CdS, CdSe, and CdTe. *Physica B* **2006**, *373*, 124–130.

10. Xin, J.; Zheng, Y.; Shi, E. Piezoelectricity of Zinc-Blende and Wurtzite Structure Binary Compounds. *Appl. Phys. Lett.* **2007**, *91*, 112902.

11. Adachi, S. *Handbook on Physical Properties of Semiconductors*; Handbook on Physical Properties of Semiconductors Bd. 2; Kluwer Academic Publishers, 2004.

12. Sasaki, K. Study on Work Function of the 0001 Faces of CdS Crystal. I. *Jpn. J. Appl. Phys.* **1974**, *13*, 933.

13. Pankove, J.; Dean, J.; Inogouchi, T.; Mito, S.; Pankove, J.; Park, Y.; Shin, B.; Tairov, Y.; Vodakov, Y.; Wagner, S. *Electroluminescence*; Topics in Applied Physics; Springer Berlin Heidelberg, 2006.

14. Pellant, I.; Valenta, J. *Luminescence Spectroscopy of Semiconductors*; Oxford Univ. Press, Oxford, 2012.